Bulk changes in semiconductors using scanning probe microscopy: nm-size fabricated structures

Shachar Richter,* Yishay Manassen,[†,‡] and David Cahen[†]

The Weizmann Institute of Science, Rehovot 76100, Israel

(Received 6 August 1998)

Hemispherical $p/n/p$ transistor structures ranging from 100 μm down to 0.05 μm in diameter are fabricated in CuInSe$_2$, by application of a high electric field between a conducting diamond tip of an atomic force microscope and a CuInSe$_2$ crystal. This leads to electromigration of Cu ions in the bulk of the material. The results of this thermally assisted process are the transistor structures. These are characterized by scanning spreading resistance microscopy. For large devices these results are compared and found to agree with those of ''conventional'' electron-beam-induced current ones. Removing several tens of atomic layers from the top surface of a structure does not affect the spreading resistance image of the device. This indicates the three-dimensional hemispherical nature of the structures. [S0163-1829(99)13515-X]

I. INTRODUCTION

Until recently, characterization of electronic devices with scanning probe microscopy (SPM) techniques was mostly an academic exercise to prove the tool's powerful ability. However, nowadays major device manufacturing industries, with the help of SPM companies, have started to adopt some of SPM's techniques as integrated tools, mainly for qualitative failure and quality analysis. Among the types of SPM used, we note atomic force microscopy (AFM) combined with scanning capacitance microscopy (SCM),[1] and recently AFM with spreading resistance microscopy (SSR).[2] Simultaneously, an effort is being made to create electronic devices with the SPM. This, however, was and is a difficult aim to achieve. Using SPM tips one can move, react, etch, and dissolve atoms of, or molecules on, surfaces, and even, in some cases, move atoms in the bulk.[3,4] The next step, namely to exploit these abilities to create a complete device structure using only SPM, was not achieved hitherto.

We have recently exploited the *nanolithography* and the *characterization* abilities of SPM and combined them to fabricate and characterize *sub-μm* diode and transistor structures, using SPM methods, in which the tip is electrically conducting. We showed that if we apply a strong and local electric field (E field) we can induce dopant diffusion in three dimensions (in the bulk and on the surface).[5]

This process can be induced in semionic semiconductors, i.e., materials in which dopants can be made mobile under conditions where they still show extrinsic semiconductivity, and takes place in addition to the mobility of the electrons and holes.[6] It is called thermally assisted electromigration (TAEM) because it is governed by the drift of the dopant due to the strong applied E field, together with the Joule heating resulting from the E-field-induced current passage.

Here we demonstrate how, by inducing TAEM of mobile dopants in crystals of CuInSe$_2$ (CIS), we can locally control the crystal's electrical conductivity type and create transistor and diode structures that vary in size from 100 μm down to 0.05 μm in different locations on the surface. This flexibility is possible due to the ability that exists in SPM techniques to control the lateral movement of the tip (with nanometer precision) and the vertical force applied to the crystal by the tip (with nanonewton control). This ability gives us a tool in which we can move an electrode (tip) to a desirable location and apply an E field through a controllable contact area. We show that it is possible to create more than one structure, by application of a series of ''isolated'' pulses, and create more than one sub-μm-sized device within a range less than 0.5 μm.

Large ($>$10 μm) homojunction devices were previously created by TAEM in p- and n-CIS. This was done by application, at ambient temperatures, of a strong E field to an initially electrically homogeneous crystal, through a metal-semiconductor contact.[7–10] When the field was removed, stable junctions with hemispherical shape remained (see Fig. 1 for a schematic view of the process). Electron-beam-induced current (EBIC) was used to demonstrate the creation of 10–100-μm-diam diode and transistorlike structures. Further studies showed that the mechanism leading to this phenomenon is TAEM of the mobile Cu$^+$ ions under the influence of the applied electric field. Similar results were obtained in Li- and Cu-doped Si and in Cd-rich (Cd,Hg)Te. These experiments demonstrated the ability to induce bulk diffusion of dopants over distances of up to hundreds of μm. These unique hemispherical structures can function as bipolar transistors with switching and amplification operation.

It became clear, however, that further miniaturization and characterization of the devices was not possible with the method described above. Not only was the minimum resulting contact diameter $\sim$1 μm, it was also not possible to get true control over the contact area, or over the extent of penetration of the tip into the surface. This seriously limits the ability to decrease the device size, for the simple reason that the device size cannot be less than the contact dimensions. In addition, the main diagnostic tool used, EBIC, cannot detect structures much smaller than 2 μm in CIS, because of the carrier lifetime and resulting carrier diffusion lengths in the material.[11] We found that we can overcome these problems, and achieve better control on the device size, if we use an AFM with an electrically conducting tip for fabrication. The problem of characterization of the devices on a nm scale is
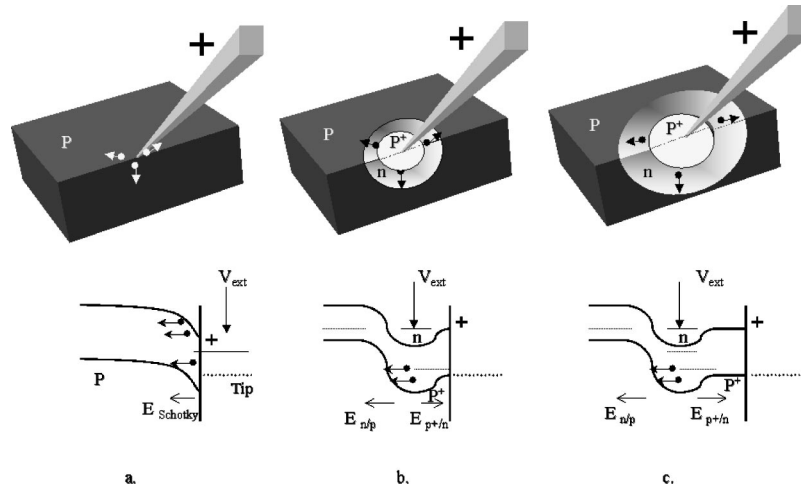
FIG. 1. Schematic explanation of the thermally assisted electromigration (TAEM) process for structure creation and propagation in $CuInSe_2$ (after Ref. 8). (a) Displacement of Cu^+ ions from the reverse biased tip-sample contact (top) and one-electron energy-band diagram, corresponding to the process (bottom). (b) Creation of hemispherical inhomogeneity in the distribution of Cu^+ ions and displacement of Cu^+ ions from the reverse biased n/p(bulk) junction. The one-electron energy-band diagram of the $p^+/n/p$ junctions that result from the process is illustrated. (c) Further propagation into the bulk of the structural inhomogeneity created by TAEM with its corresponding one-electron energy-band diagram.

solved by using the conducting AFM tip as one of the electrodes for electrical characterization. Characterization of the structures can be done using different SPM-based techniques, SSR and SCM methods.

We will show that in the case of the SSR technique, where the contact is established by an elastic deformation of a sample by a diamond tip, the local resistance depends on the sample electrical properties and on the mechanical properties of the tip and the sample. De Wolf et $al.$[2] have demonstrated that one can characterize, both qualitatively and quantitatively, semiconductor devices using SSR. They used layered or sandwiched devices, every section of which is directly connected between the two electrodes which measure the resistance. In the case of the hemispherical, TAEM-created device structures this is not possible. The reason is that electrical configuration of the structure between the two measuring electrodes (the back contact and the AFM tip) is not the same in different regions of the device.

Far from where the device is created, the configuration is $electrode/p$-$type/electrode$ ($e/p/e$); near the center of the structure, the configuration is $e/n/p/e$ and in the center it is $e/p^+/n/p/e$ (see Fig. 1). Thus the assumption that the spreading resistance condition occurs, namely that the main resistance is the surface-tip one, needs to be proven. The agreement between SSR and EBIC images of large device structures (20 μm diam), created by AFM, showed that this is indeed the case. The question of the SSR contrast is discussed quantitatively below.

II. EXPERIMENT

n-$CuInSe_2$ single crystals were grown by the traveling heater method (THM) (see Ref. 12 for details). Structurally they were characterized by x-ray Laue diffraction and in terms of chemical composition by electron-beam-induced, energy-dispersive x-ray fluorescence spectroscopy measurements. Conversion of crystals to p-type was done by annealing in Se vapor for 20–40 min at 600 °C. The physical and

electrical properties of the samples were checked by four-probe resistance and Hall effect measurements with the van der Pauw configuration. Experiments were done on smooth surfaces that had been freshly cleaved in air or N_2. A commercial AFM, operating in N_2 atmosphere, was used to fabricate and characterize the device structures.[13]

EBIC images of the large structure were obtained with the standard procedures.[14] CIS samples with a contact were negatively or positively biased with respect to the positive or negative AFM tip, respectively, in either of the following modes: (i) for the large structures a unipolar trapezoidally changing voltage was applied at a frequency of up to 45 Hz; (ii) sub-μm structures were created using a single pulse, -2 to -10 V sample bias in amplitude, for 0.05–0.1 sec. Below we show how these two modes differ in terms of their effect on the process parameters.

The AFM tip used in the experiments was an electrically conducting (doped) diamond one with radius less than 20 nm.[15] The ability of working with one tip for several months (because it is not composed of a coated material and could be cleaned easily), its relatively high electrical conductance, and the possibility to apply high electric fields and currents made this the most suitable type of tip, despite its high cost.

Home-built systems for E-field application for SSR were used to fabricate and characterize the devices (see Fig. 2 for the experimental setup). This modular configuration equipped with low capacitance and electrical noises enabled us to switch from the E-field application system to the characterization one without significant drift and thus to explore the structure after its fabrication.

III. RESULTS AND DISCUSSION

Shrinking the device size

Figure 3 shows AFM and SSR images of device structures, created by AFM, ranging from >100 μm down to the submicron region. The topography and the SSR images were
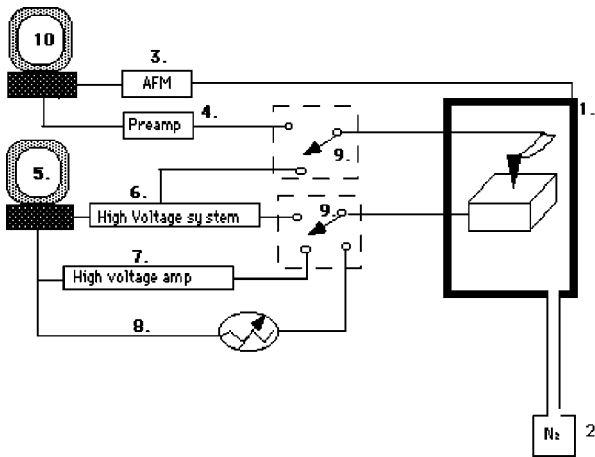
FIG. 2. Experimental setup: (1) AFM equipped with an electrically conducting diamond tip operated in N_2 atmosphere is used as part of a combined AFM-SSR system (3 and 4) and to a programmable voltage supply for the trapezoidal, single, and SSR modes (6, 7, and 8, respectively). The systems are computer controlled (10 and 5) and connected via low capacitance remote switches (9).

FIG. 3. Topography and SSR images of structures from 100 μm down to sub-μm size. The images are collected simultaneously after application of the E field. In all the figures n type appears as white, p and p^+ as black. (a) Images of large structure ($>$100 μm) made by applying the E field to a polished surface. The scratch and the hole were created while applying -50 V sample bias(max) trapezoidal voltage. In addition to the expected structure of the transistor which appears partially in the SSR images, some black channels appear, indicating line defects. (b) Application of -25 V sample bias to a cleaved CIS sample in the trapezoidal mode results in a 40 μm structure. The internal electrical features of the structure are somewhat shaded due to the contamination that can be seen in the topographical image. The steps of the cleaved surface do not influence the (electrical) structure of the device. (c) Application of single -5 V sample pulse resulted in a 0.5 μm structure. The p^+, p, and the n regions are clearly imaged in the SSR image.

taken simultaneously after application of the E field. For the large structures [Figs. 3(a) and 3(b)] the trapezoidal voltage method was used and for the sub-μm structures a short single voltage pulse was applied.

The topography mode of the AFM reflects the surface corrugations of the crystal. The CIS crystal in Fig. 3(a) was polished (the polishing scratches are imaged), while the CIS surface images in Figs. 3(b) and 3(c) are cleaved ones (notice the steps on the smooth surface). It is obvious that the polished surface is unsuitable for creating regular structures, because it is not as smooth and well-defined as the cleaved surface. This causes a high degree of unpredictability in the electric field distribution and in the subsequent dopant drift.

The SSR images reflect the surface resistance. The gray scale in the image is proportional to the conductivity (white: more conductive; black: less conductive). In all of the SSR images white corresponds to n-type regions and black to p and p^+ areas. We found the n type shows higher conductivity than p-type areas. This is due to the higher mobilities of the electrons compared to the holes in CIS.

Prior to further analysis we need to check to what extent we can distinguish between topographical and electrical features. When we have identical features with curvatures that are somehow similar in the SSR and the topography modes, it is necessary to check whether it comes from ''topographical transformation'' of data from the topography image to the SSR one,[16] or if the SSR image is a real projection of the sample's electrical properties. Notice that in the structure in Fig. 3(c), hardly any of the topographical features can be related to the SSR images. This is generally the case in the submicron devices.

Figure 3(a) shows a structure which is larger than 100 μm in diameter. Due to the limited range of the AFM scanner, the p-conductivity part could be explored only partially (it appears in the upper left area of Fig. 3 in the SSR image). The hole and the scratch that are shown in the topography mode in Fig. 2(a), which were generated during the voltage application, could not be related to the SSR image, especially to the regions which are far from these topographical fea-

tures. Furthermore, the unusual black lines in the SSR image are not imaged in the topography one. This could be due to the existence of subsurface dislocations, along which pipe diffusion may occur. This could explain the observed local changes in the conductivity.

The spherical SSR image (which is a projection of the hemispherical structure) is shown in Fig. 3(b). Notice that although the contamination at the center of the structure affects the SSR image (the p^+ area is shaded) there is no one-to-one correspondence between the topography and the SSR image. Moreover, the steps which appear in the topography image do not change the structure of the device. This implies that the surface diffusion of the dopant can be neglected and the process can be treated as a bulk diffusion phenomenon.

When approaching the sub-μm regions, the undesirable damage, if created, cannot be neglected because the size of it can be comparable to the size of the device itself. Therefore, for sub-μm device structures, we have not considered further
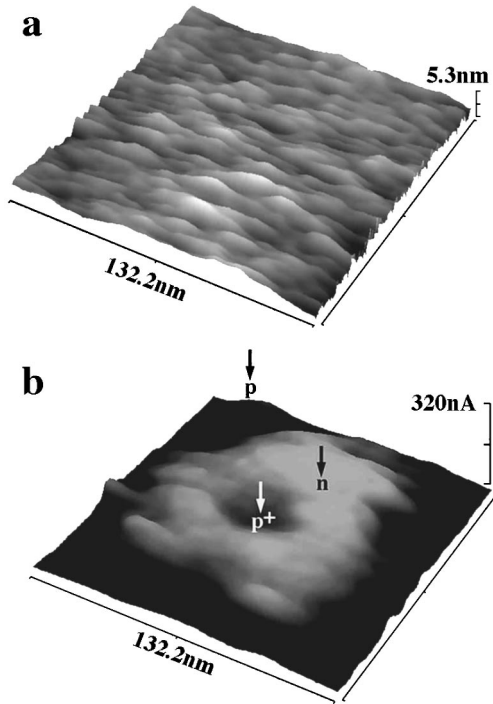
FIG. 4. (a) SSR image of a 90 nm transistor structure. The ''bagel''-like SSR image is a surface projection of the hemispherical structure illustrated in (b).

any structure with such defects. Examples for some sub-μm structures are shown in Figs. 3(c), 4, and 5.

Figure 3(c) shows a 0.5 μm transistor structure in which the internal features are explored. The different conductivity areas are shown. Although some damage is done during the fabrication process, it is clear that the SSR image is not a topography projection, and the round structure of the device is not connected to the topography image.

By using this method we can approach the lower limits of these structures, which are $\sim$10 times the Debye length, L_D (approximately 70 nm—as discussed in Ref. 5), as demonstrated in the SSR image by a 90 nm double transistor structure [Fig. 4(a)].
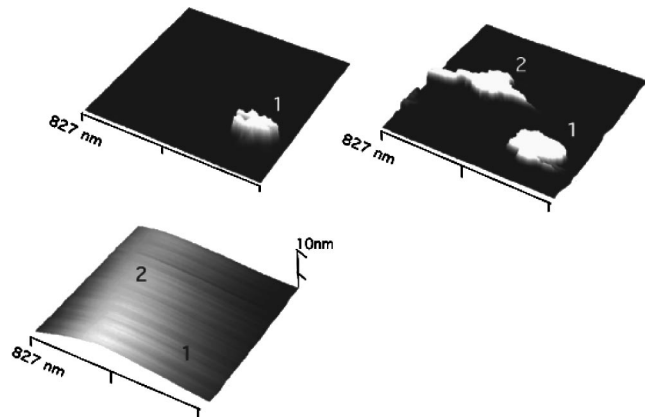
FIG. 5. Application of two successive short pulses resulted in two sub-μm structures at locations 250 nm apart. (a) SSR image showing the area after application of the first pulse; (b) SSR image showing the area after application of the second pulse; (c) AFM topography image of the area after application of the second pulse. No damage can be seen.

The ability of SPM to locate a tip within a precision of angstroms can be used for fabrication of more than one device structure. Figure 5 illustrates the creation of two 200 $\times$ 100 nm device structures (the internal features could not be imaged). Figure 5(a) shows the SSR image of a structure which was generated after application of -5 V (sample bias) for $\sim$10 msec. Fabrication of a second device which is located only 250 nm from the first one was done by application of a successive pulse with the same parameters to the desired location. Figure 5(b) shows the SSR image of the area, featuring the two structures. The topographic image of the area after the generation of the two structures is shown in Fig. 5(c). The location of the two structures is labeled. The absence of physical damage is clear.

Controlling the device size

Important questions to be asked are what are the parameters that influence the size of the device and to what extent are they controllable?

We can identify three main factors that influence the process: (i) the structure of the voltage pulse, (ii) the physical properties and structure of the sample, and (iii) the physical properties and the shape/size of the tip. The electrical pulse naturally induces two processes in parallel: thermal diffusion induced by Joule heating and E-field directed drift of dopants. Therefore it is important to be able to estimate the temperature and the temperature gradient, as well as the effective electric field during the process.

The evaluation of the temperature during a single pulse process and during a process induced by a series of pulses is different. In a single pulse experiment the temperature increment is expected to remain constant during the pulse duration t_1 and to decrease exponentially after the pulse is stopped. Thus

$$\Delta T(\text{pulse}) = \frac{0.5P}{\pi k_{\text{th}}R_0}, \tag{1}$$

where ΔT (pulse) is the average temperature rise above room-temperature change during the pulse from time t to the end of the voltage pulse, t_1, P is the average electric power dissipated in the sample, k_{th} is the CIS thermal conductivity, and R_0 is the tip radius.

The relaxation temperature T_{rel} from temperature T_1 at time t_1, after the pulse is stopped, can be estimated as

$$T(\text{rel}) = T_1 \exp\{-[(1-t)/\tau]\}, \tag{2}$$

where T_1 is the average temperature after the pulse is stopped and τ is the relaxation time. After the pulse is stopped and the temperature has decreased to ambient, a new state in which the dopants are redistributed is established. However, the situation is different when a series of pulses is applied to the sample. Two types of pulses can be applied: (i) The duration time between pulses, t_D, is less than the relaxation time τ; (ii) $t_D > \tau$. The temperature distribution in case (i) will be different from case (ii). In case (i) the system is not in a steady state and has some initial temperature, while in case (ii) the system was cooled down. There-

TABLE I. Parameters which influence the fabrication and characterization of the CIS small structures (see text).

Parameter	Demands	Influence	Controllable
Tip radius and shape	Large aspect ratio, sharp tip	Contact area, electric field distribution, temperature change and gradient, SSR resolution	Very hard to make (or purchase) tips with identical radius and structure.
Tip force constant	High (for better contact)	Contact area	Available
Tip material	Hard, electrically conducting, not influenced by heat, inert	Contact area, electrical conductivity, reproducibility, contamination of the surface and the tip	Yes (diamond tips are available)
Sample electrical properties	High carrier concentration (small Debye screening length is necessary for small devices).	Minimum device size	Partially; harder to control carrier concentrations in CIS than in ''classical'' semiconductors
Sample chemical and mechanical properties	Avoid phase separation, due to concentration changes. Low concentration of defects. Smooth surface	Size and shape of the device, reproducibility	Yes
Sample mechanical properties	The elastic modulus should be as large as possible (hard material)	Contact area, plastic deformation	In principle yes; CIS is a relatively soft material
Pulse duration time structure and amplitude	Versatility: from μsec to seconds pulse duration time, from mV to 50 V magnitude, different pulse structures, current limit	Electric field distribution and magnitude, temperature change and gradient, diffusion coefficient, and mobility	Yes
Environment	Inert environment (N_2)	Competitive processes: Redox processes, other chemical reactions on the surface	Yes

fore, it seems that application of a series of pulses in the form of (ii) will enable us to control the size of the device more effectively.

Nevertheless, application of a single pulse differs from application of a series of pulses in the form of case (ii). The first difference is the distance over which the dopant will drift and diffuse, which is proportional to the time of pulses. Thus application of n pulses with total time (nt) will result in a larger device than that of a single pulse with time t. A more basic difference is that of initial conditions: If a single pulse is applied, the process is finished after the relaxation takes place, and a kinetically stable system is established. However, this is not the case when a series of pulses is applied. Due to the existence of inhomogeneous dopant profiles and internal electric fields, generated after a previous pulse, the initial conditions in terms of carrier distribution and internal forces (fields) are different for each pulse. For example, creation of the $p^+/n/p$ configuration will lead to an electric force which is directed opposite to the diffusing positively charged ions (the p^+/n built-in electric field), and to a force which is in the direction of the diffusing Cu^+ (the n/p built-in electric field).[21] Therefore, we can conclude that a single pulse is the most favorable mode to control and mini-

mize the device size. For large device application we can use multiple pulses in mode (i) or (ii).

However, we found it difficult then to control the device size and to relate it to the experimental parameters. This is due to the complexity of the system. In addition to the pulse factors, the characteristics of the sample and the tip (material factors) influence the processes of fabrication and the electrical characterization. A summary of the parameters that may affect the device size and its characteristics is given in Table I. The ability to control the parameters is introduced in the table.

From Table I it can be concluded that the two main material factors governing the ability to control the process are the chemical and electrical properties of CIS and the contact area. Although much progress has been made over the past ten years in the field of CIS crystal growth and doping,[12] it is still hard to grow crystals in which the defect and carrier densities are fully controlled. Thus, if we have samples with different physical and chemical parameters it is obvious that for every sample the device fabrication and characterization conditions will be different. Furthermore, we found that within a single crystal it is hard to create two identical devices. This could be due to inhomogeneity in the crystals or

due to the inability to keep the contact area constant. As far as the former possibility is concerned, EDS data show the crystals to be homogeneous within the limited accuracy of that method, as do careful synchrotron single-crystal x-ray-diffraction experiments. However, in all those cases only average properties are measured (μm's for EDS, ~0.1 mm for XRD).

The contact area depends on many factors, but mainly on the load on the tip and on the tip radius. Assuming that the tip radius is not changed, we conclude that the contact area is changed due to the fluctuations of the external load on it. The reasons for it could be poor reflection from the cantilever or heat transfer during the pulse from the diamond to the stainless-steel cantilever.

We conclude that although it is possible to fabricate these devices down to the sub-μm sizes, it is still hard to control their size and to relate it to some physical parameters due to the inability to control some of the factors involved in the process. Silicon doped with mobile ions such as Li or Cu seems to be a promising system to investigate, due to the existing technology which allows fabricating silicon crystals with controlled density of defects and smooth surfaces.

Comparison between the SSR and EBIC modes

Since we attempt to characterize the sub-μm structures with the SSR, we have to prove the capability of this characterization technique to distinguish between areas with different conductivity types. This is furthermore necessary because the standard spreading resistance and nano-SSR methods[2] are designed and used for characterizing traditional electronic devices which differ significantly in shape and size from our structures. In addition it is not possible to claim that what we observed is pure spreading resistance. The difference in Schottky barrier between the tip and the surface in the n and p regions, respectively, is expected to modify the local SSR. For this reason it is important to show that, nevertheless, the qualitative value which was observed in the measurement correctly reflects the local conductivity type in this material. Our basic approach was to compare the SSR image of a ''large'' (15–30 μm) device to its EBIC image. EBIC is a well-established technique to investigate these devices.[7–10] Based on such a comparison we can then use SSR to characterize devices that are too small for EBIC characterization.

Application of the unipolar trapezoidal mode (with low average amplitude larger than 10 V) yielded device structures with sizes of 20–200 μm. Secondary electron (SE) and mixed SE and EBIC (SE/EBIC) images are shown in Fig. 6, along with the AFM topography and conductivity images. Contrast corresponding to p-n diode structures is clearly seen in the EBIC images. The corresponding scanning spreading resistance images yield white contrast on a dark background, where white represents n- and black p-type doping.

The AFM topography [Fig. 6(d)] shows that, although applying the pulse resulted in slight surface damage, its size is much smaller than the extent of the device structure, shown by SSR contrast. Figure 6(e) shows a bright central region, surrounded by a fainter halo representing the transition from n to p^+. The bright appearance at the steps could be due to a change in the tip-sample contact area (topo-
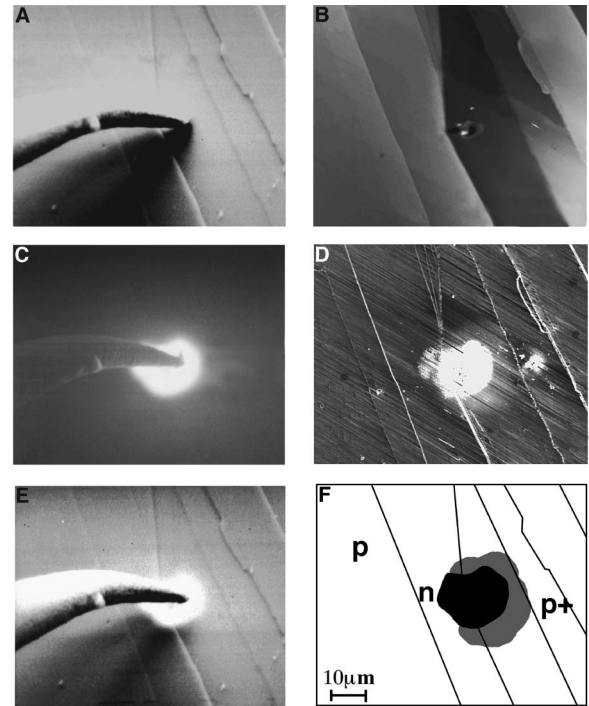
FIG. 6. 25 μm diode structure created by application of +15 V sample bias, using a periodic, trapezoidal voltage shape. (a) Secondary electron image, showing the metal tip used for simultaneous electron-beam-induced current (EBIC) measurements; (b) EBIC image; (c) mixed secondary electron and EBIC image; (d) AFM topography of the same area; (e) scanning spreading resistance image; (f) sketch of the device structure, indicating step structure as measured by the two techniques. Note that there is no correlation between minor topographic damage and the SSR image.

graphical enhancement), or to a true increase of the conductivity at the steps, relative to the terraces. Additional defects and the small device structure to the right of the large one, which appear in Fig. 6(e), are not seen in Fig. 6(b), because EBIC contrast is seen best when there is direct contact between the tip and the device.[7] Comparison of the EBIC with the SSR image of the same structure shows one-to-one correspondence.

From the agreement between the SSR and EBIC images on the large device structures, we conclude that the SSR method can be used to characterize submicron device structures, which are beyond EBIC resolution.

Bulk versus surface phenomena

SPM techniques are considered to be sensitive to the surface character and not to the bulk ones. Thus, the interpretation that we image a projection of a bulk process on a surface [Fig. 4(b)] needs to be examined. Unfortunately, in contrast to what we could do for the larger device structures (cf. Ref. 7), there is no way by which one can show the three-dimensional nature of the process, illustrated in Fig. 4(b), directly. Therefore we used a different approach.

Figure 7 shows an SSR image of a 10 μm transistor structure after removal of some parts of it. After the device was created some of the topmost layers of the material (approximately 20 nm as measured by the AFM topographic mode, using the step as a scale) were removed using the diamond
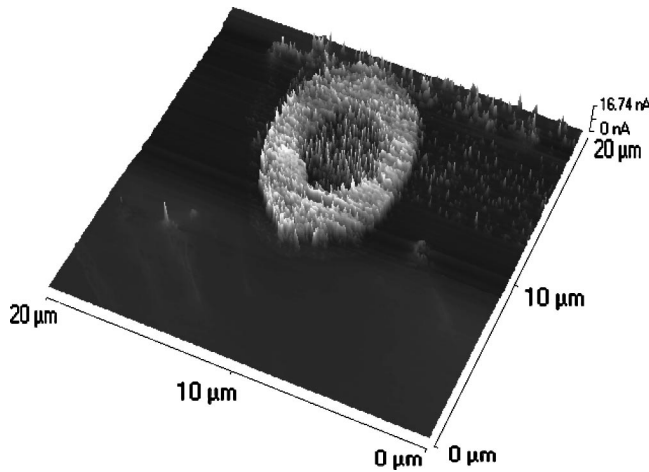
FIG. 7. SSR image of a 10 μm transistor structure after removal of 20 nm of the uppermost layers. The basic structure of the transistor has not been affected.

tip. Arrows label the area from which the material was removed. Despite the fact that this method of removal might be a little unreliable, still it is the most convenient method for local removal of material. The resulting image must be interpreted with caution. However, one can see from the SSR image that although the signature of the ''sweeping'' action is seen in the image as spikes indicating instability in the resistance, it did not change the basic oval shape of the device structure which is seen clearly. This provides support to our expectation that the SS image is a surface signature of a bulk structure that extends to the surface.

Contrast mechanism in the SSR mode

Although we found a similarity between the EBIC and the SSR images, it is important to stress that while EBIC contrast is based on a current generated due to separation of electron-hole pairs in regions where an internal electric field is located (p-n junctions in our case), in SSR this is not the case. We can estimate the origin of the SSR as follows.

The resistance of the contact can be estimated from the spreading resistance theory[17] as

$$R = \frac{\rho}{4}\left(\frac{\pi}{A}\right)^{1/2}, \tag{3}$$

where ρ is the local resistivity and A is the contact area.

A in our experiment can be estimated using a Herzian model[18] in which we assume that the diamond tip is not changed during the contact. Thus

$$A \approx \left[\left(\frac{3N(1-\nu)}{8E}\right)^2 \frac{1}{r}\right]^{1/3} r, \tag{4}$$

where r is the tip radius (in cm), N is the force applied by the tip (in N), and E and ν are the Young modulus and the Poisson ratio of the sample, respectively. Substituting $N = 50$ nN (from AFM measurements), $\nu = 0.25$,[20] $r = 20$ nm (obtained from SEM measurements), and $E = 50$ Gpa (Ref. 19) in the equation gives $A \sim 10^{-16}$ m^2 and thus for R in the range of $M\Omega$ (for $\rho = 1\,\Omega$ cm, which is the average value found for p-type samples). This value is larger than any resistance in the system, and therefore the spreading resistance mechanism is valid. The current measurements are then proportional to the local resistivity of the sample which scales with the local electrical properties as

$$\rho_{n,p} = \frac{1}{qn(p)\mu_{n,p}}, \tag{5}$$

where $\rho_{p,n}$ are the local resistivities of the p and the n regions, respectively, n (p) is the carrier concentration of the n (p) area, and $\mu_{n,p}$ is the mobility of the majority carriers. Hence, the current images of the small and large device structures are directly related to the change in the local doping concentrations and to the carrier mobilities of the samples. These were measured in our samples to be an order of magnitude larger for electrons than for holes, resulting in higher conductivity for n than for p type.

Summary

We have demonstrated how, by inducing TAEM of mobile dopants in crystals of CIS, we can change the crystal's electrical properties locally and create double transistor and diode structures that vary in size from 100 μm down to 90 nm. The characterization technique, SSR, is compared to the EBIC one and proven to be suitable for characterization of such structures, also below the size limit where EBIC can be used.

ACKNOWLEDGMENTS

*Present address: Lucent Technology, Bell Labs, Murray Hill, NJ 07974. Electronic address: shachar@physics.bell-labs.com

†Authors to whom correspondence should be addressed. Electronic addresses: cscahenl@weizmann.weizmann.ac.il, manassen@bgumail.bgu.ac.il

‡Present address: Dept. of Physics, Ben Gurion University of the Negev, P.O. Box 653, Be'er Sheva, 84105, Israel.

[1] A. Erickson, L. Sadwick, G. Neubauer, J. Kopanski, D. Anderton, and M. Rogers. J. Electron. Mater. **25**, 301 (1996).

[2] P. De Wolf, T. Clarysse, and W. Vandervorst, J. Vac. Sci. Technol. B **16**, 320 (1998).

[3] A. Utsugi, Nature (London) **347**, 747 (1990).

[4] A. Sato and Y. Tsukamato, Nature (London) **363**, 431 (1993).

[5] S. Richter, V. Lyakhovitskaya, S. R. Cohen, K. Gartsman, D. Cahen, and Y. Manassen, Appl. Phys. Lett. **73**, 1868 (1998).

[6] D. Cahen, in *Ternary and Multinary Compound*, Proceedings of the 7th International Conference (Materials Research Society, Pittsburgh, 1987).

[7] D. Cahen, J. M. Gilet, C. Schmitz, L. Chernyak, K. Gartsman, and A. Jakubowicz, Science **258**, 271 (1992).

[8] K. Gartsman, L. Chernyak, J.-M. Gilet, R. Triboulet, and D. Cahen, Appl. Phys. Lett. **61**, 2428 (1992).

[9] L. Chernyak, K. Gartsman, D. Cahen, and O. M. Stafsudd, J. Phys. Chem. Solids **56**, 1165 (1995).

[10] D. Cahen and L. Chernyak, Adv. Mater. **9**, 861 (1997).

[11] Monte Carlo simulations [based on a program written by E. Napchan, cf. E. Napchan, Rev. Phys. Appl. **24**, 15 (1989)] of an EBIC signal were performed to estimate the resolution.

[12] V. Lyakhovitskya, S. Richter, L. Kaplan, Y. Manassen, K. Gartsman, and D. Cahen, J. Cryst. Growth **197**, 177 (1999).

[13] We used a Topometrix TMX2010 Discoverer AFM.

[14] Philips 515 SEM. Standard working conditions for EBIC were 30 kV accelerating voltage 100 nm spot size and 0.5–1 nA beam current.

[15] Conducting diamond tip for AFM (R-Dec Co., Ltd, Japan).

[16] S. Richter, Ph.D. thesis, Weizmann Institute of Science, 1998.

[17] H. K. Henisch, *Semiconductor Contacts: An Approach to Ideas and Models* (Clarendon, Oxford, 1984).

[18] The Herzian model assumes that in the contact mode no adhesion or surface forces act in addition to the electrostatic repulsion force exist. For AFM contact area calculation using the Herzian model, see S. R. Cohen, G. Neubauer, and G. M. McClelland, J. Vac. Sci. Technol. A **8**, 3449 (1990).

[19] *Narrow Gap Cadmium-based Compound*, edited by P. Capper (Inspec, London, 1994). The values were obtained from data for CdTe, which has mechanical properties similar to CIS, and from nanomechanical AFM measurements (Ref. 16).

[20] Since exact measurements are needed for determination of the Poisson ratio, it is assumed for most common materials as 0.25. See J. E. Boyd, *Strength of Materials* (McGraw-Hill, New York, 1935).

[21] R. J. Borg and G. J. Diens, *An Introduction to Solid State Diffusion* (Academic, CA, 1988).